



IUTAM Symposium on Multiphase flows with phase change: challenges and opportunities,  
Hyderabad, India (December 08 – December 11, 2014)

## Dynamics of collapse of free surface bubbles

Krishnan Sangeeth<sup>a</sup>, Baburaj A. Puthenveetil<sup>a</sup>

<sup>a</sup>Department of Applied Mechanics, IIT Madras, Chennai, 600036, India

---

### Abstract

We experimentally study the collapse of cavities formed by bubbles of different radius  $R$  at the free surface of five different fluids. The tangential and normal velocities of the disturbance front on the bubble surface were measured and shown that the tangential velocities scale as the capillary velocity  $(\sigma/\rho R)^{1/2}$ . The total time for the completion of cavity collapse was measured and shown to scale as capillary time scale  $R^{3/2}/(\sigma/\rho)^{1/2}$ . We hence infer that the cavity collapse is dominated by surface tension and inertia with viscosity not playing a role in the regime of our investigation. Such a behavior of cavity dynamics is different from the behavior of jet velocity discussed by Sangeeth et.al.[9] wherein the jet velocity showed a clear viscous cut off. The rate of change of cavity volume was found to be constant with time, the implications of which needs to be investigated further.

© 2015 The Authors. Published by Elsevier B.V. This is an open access article under the CC BY-NC-ND license (<http://creativecommons.org/licenses/by-nc-nd/4.0/>).

Peer-review under responsibility of Indian Institute of Technology, Hyderabad.

*Keywords:* cavity collapse; bubble; jets

---

### 1. Introduction

Bursting of bubbles at free surfaces occur frequently in nature. The nearly spherical cavity, formed after the rupture of the thin film cap, collapses and results in the convergence of an axisymmetric flow to the bottom of the cavity, resulting in a fast moving jet. The Reynolds number  $Re = \rho V_j R / \mu$  of the cavity collapse is of the order of 1000. The high inertial focusing at such large  $Re$  compelled earlier researchers to consider the phenomenon as free from surface tension mediation [6]. The process, which completes within a fraction of a second, results in the fragmentation of the jet into different sized drops. In addition to this, the thin film cap, produces tiny droplets after rupture [7, 8], which evaporates into the outside air. So the bubble bursting process plays a significant role in the transport of water particles across ocean surface. This bursting process also plays an important role in damaging bacterial cells in bio-reactors [1]. The collapsing of the bubble cavity is fascinating especially because it is thought to include finite time singularity and could be analogous with other physical singularities such as standing wave

collapse [10]. However, in standing wave collapse, which yields fast jet after collapse, Zeff et. al [10] and later Das and Hopfinger [3] have established the role of surface tension and viscosity.

The bubble breakup process at free surface was experimentally studied by Kientzler [5] using high speed photographic techniques. MacIntyre [8] later interpreted Kientzler's [5] data, after augmenting the data with that from his experiments using dyed bubbles, and proposed the driving mechanism as a boundary layer flow along bubble cavity which causes stagnation pressure at the bottom of the cavity. Boulton-Stone and Blake [1] calculated jet velocities from bubble collapse at an air water interface for the range of bubble radii  $0.5\text{mm} < R < 3\text{mm}$  using boundary integral method; their data shows that the jet velocity varies as  $1/R$ . Duchemin et al.[4] performed numerical simulations and found jet velocities for a wide range of bubble sizes,  $1.4\mu\text{m} < R < 20\text{mm}$ . Three distinctive regimes were seen by Duchemin et. al. [4] for water:  $R > 0.5\text{mm}$ , the jet velocity  $V \sim 1/R^{1/2}$ , for  $0.012\text{mm} < R < 0.5\text{mm}$ ,  $V \sim 1/R$  and for  $R < 0.012\text{mm}$   $V$  decreased with  $R$ . Hence, the numerical simulations of [1] and [4] differ about the scaling of jet velocity as a function of bubble radius, when  $R > 0.5\text{mm}$  in water.

Our experimental studies [9] with fluids of different viscosities and surface tensions found that the jet velocity varied as  $1/R$  when  $R/R_v > 10^3$ , unlike the  $1/R^{1/2}$  scaling found by [4]. We had also observed a viscous cut off for the jet velocity dependence on  $R$  around  $R/R_v \approx 10^3$ , with the jet velocity showing an increase with increase in bubble radius when  $R/R_v < 10^3$ . The jet formation is an outcome of the cavity collapse. We have to hence understand the physics of cavity collapse for a better understanding of jet formation in bubble collapse at free surfaces. In this paper, we hence study the dependence of variables that describe the cavity collapse on the radius of the bubble  $R$ .

### Nomenclature

$\sigma$	surface tension	$\nu$	kinematic viscosity
$\rho$	density of the fluid	$\mu$	viscosity of the fluid
$R$	radius of undeformed spherical bubble	$t_{tc}$	total time of cavity collapse
$V$	jet velocity at free surface	$V_t, V_n$	tangential, normal components of cavity collapse
$R_v$	viscous- capillary length scale. $\rho\nu^2/\sigma$	$Q_t, Q_s$	total, side wise filling rate of cavity
$V_v$	viscous – capillary velocity $\sigma/\rho\nu$	$V_\sigma$	capillary velocity $(\sigma/\rho R)^{1/2}$
$t_v$	viscous – capillary time scale $\rho^2\nu^3/\sigma^2$	$t_\sigma$	capillary time scale $(\rho/\sigma)^{1/2} R^{3/2}$
$R_r$	rim radius	Oh	Ohnesorge number $\mu/(\sigma\rho R)^{1/2}$
Bo	Bond number $\rho g R^2/\sigma$	$l_c$	capillary length $(\sigma/\rho g)^{1/2}$
Re	Reynolds number $\rho V_r R/\mu$	$R_d$	arc radius of cavity surface

## 2. Experimental setup and methodology

The collapse of bubbles at the free surface and the subsequent jet formation were studied using the set-up shown in Fig 1 for the following fluids: water ( $\mu = 1.005\text{ mPa sec}$ ,  $\sigma = 72\text{ mN/m}$ ,  $\rho = 1000\text{ kg/m}^3$ ), 68 % glycerol-water mixture ( $\mu = 12.41\text{ mPa sec}$ ,  $\sigma = 66\text{ mN/m}$ ,  $\rho = 1170\text{ kg/m}^3$ ), and 72% glycerol-water mixture ( $\mu = 16.6\text{ mPa sec}$ ,  $\sigma = 63.6\text{ mN/m}$ ,  $\rho = 1181\text{ kg/m}^3$ ), 2-proponol ( $\mu = 2.073\text{ mPa sec}$ ,  $\sigma = 18.3\text{ mN/m}$ ,  $\rho = 781\text{ kg/m}^3$ ) and ethanol ( $\mu = 1.144\text{ mPa sec}$ ,  $\sigma = 22.39\text{ mN/m}$ ,  $\rho = 789\text{ kg/m}^3$ ). The experiments were done in a transparent acrylic tank of  $3.5 \times 5\text{cm}^2$  cross sectional area, fixed on a leveling board, which was filled up to the brim to avoid meniscus. Glass capillary tubes of different sizes were used to produce bubbles of sizes  $0.42\text{mm} < R < 4\text{mm}$  inside water by pumping air into the capillaries by a syringe pump running at a constant discharge. The discharge was selected to be within the periodic dripping regime specified by Clanet and Lasheras [2] as well as to avoid merging of bubbles due to crowding of bubbles at the free surface. Care was taken to fix the capillaries in the same way throughout the experiment to avoid variations in bubble sizes. The bubbles released from the capillary stay at the free surface for a short time and burst to give rise to a vertical jet. This bursting process was captured by a high speed CCD camera at frame rates  $< 19000\text{Hz}$  using high intensity LED back lighting. A grid was placed on the back-wall of the tank to account

for the lateral shift and magnification produced due to differential refraction of light rays in liquid and air. The room temperature was kept at 20°C for all the experiments with water, while the experiments in glycerol-water mixtures were conducted at 30°C to avoid variations in viscosity at lower temperatures. Care was taken not to contaminate the interface by changing the liquids after each trial.

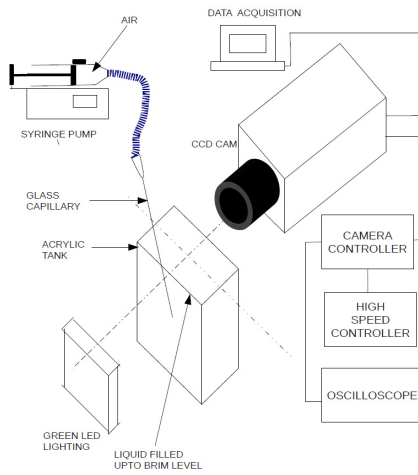


Fig 1: Schematic of the experimental set up

Experiments with propanol in the acrylic tank resulted in the liquid climbing over the sides of the tank and draining out due to its high wetting of the acrylic surface. These experiments were hence conducted in a glass petri dish of diameter 40mm and depth 11mm. The azimuthal symmetry of the container held the free surface in a slightly convex shape resulting in no drainage from the edges. In these experiments, the undeformed bubble radius ( $R$ ) was measured by counting the number of bubbles produced in 5 minutes to get an estimate of  $R$  from the discharge and comparing this with the  $R$  calculated from the measured rim radius ( $R_r$ ) by the static force balance given by Sangeeth et. al [9]. Free surface bubbles were also allowed to merge to increase the range of bubble sizes in these experiments. Experiments with ethanol were conducted in a glass tank with square cross section (5 cm x 5 cm) since drainage did not occur from the sides.

Fluid	$R$ (mm)	$Bo$	$Oh$	$l_c$ (mm)
Water	0.4 - 4.1	0.022 – 2.29	0.0018- 0.0059	2.7
GW 68%	0.48 – 2.3	0.041 – 0.92	0.029- 0.064	2.4
GW 72%	0.59 – 3.6	0.063 – 2.36	0.032- 0.079	2.3
2-propanol	1 – 2.3	0.42 – 2.21	0.011- 0.017	1.5
Ethanol	0.19 – 1.2	0.013 – 0.5	0.008 -0.02	1.7

Table 1: Range of parameters for the different fluids used.

### 3. Results and discussion

Fig 2 shows the sequence of collapse of the free surface bubble in water. The following stages could be noticed. The film drains and ruptures (Fig 2(b)) creating a circular top part of the cavity called the rim; we consider this stage as the starting point of the cavity collapse. The cavity created by film rupture, which is open to atmosphere at the top, is unstable and soon undergoes shape transition to merge with the undisturbed free surface in milli seconds, creating a jet in this process (Fig 2 (q)). The retraction of the rim results in a propagating disturbance along the cavity surface. Behind the disturbance front, the curvature is convex, while ahead of it the curvature is concave, as seen from within the cavity. The extent of the concave part decreases with time and the radius of the convex part increases till the cavity surface becomes approximately conical (Fig 2(m)); we consider this as the end of the cavity

collapse since a jet is expected to be initiated just after this stage. We now look at the scaling of the velocities of this disturbance front.

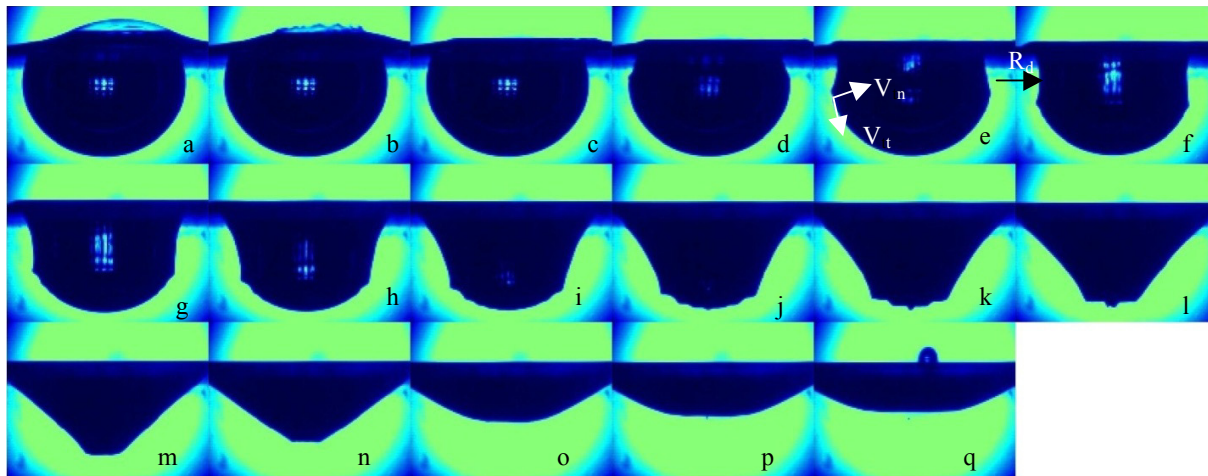


Fig 2: The bursting sequence of a bubble of radius R=2.15mm in water. Each image is separated by 0.25 msec. The whole process up to jet emergence at the free surface took 4.25 msec.

3.1. Velocity of the disturbance front

The displacements of the disturbance front between all successive images were measured and then resolved into displacements in the tangential and normal directions to the undisturbed cavity, i.e. to the cavity surface just ahead of the disturbance. These displacements were added up to get the corresponding tangential and normal location of the disturbance front with time.

The tangential distance travelled by the disturbance front was found to be linear with respect to time for all the fluids for a given radius of the bubble, implying that the disturbance front travels along the cavity surface with a constant velocity for any given radius and fluid. Fig 3 shows the variation of this constant tangential velocity  $V_t$  with the bubble radius in dimensionless form. Here,  $V_v = \sigma/\rho\nu$  and  $R_v = \rho\nu^2/\sigma$  are the viscous- capillary velocity and length scales [4]. The dimensionless tangential velocities scale as

$$\frac{V_t}{V_v} = 6 \left(\frac{R}{R_v}\right)^{-1/2} \text{ ---- (1)}$$

which also implies that  $V_t = 6 V_\sigma$ , as shown in the inset (i) of Fig 3, where  $V_\sigma = \sqrt{\frac{\sigma}{\rho R}}$  is the capillary velocity.

The normal velocity of the disturbance front had two regimes; in the initial part of the disturbance propagation  $\frac{V_n}{V_v} = 11.44 \left(\frac{R}{R_v}\right)^{-0.77}$  as shown in Fig 3. As shown in the inset (ii) of Fig 3, as  $\frac{V_n}{V_\sigma} = 4.96 \left(\frac{R}{l_c}\right)^{1.57}$  in latter part of propagation of the front; this scaling has to be verified further since the number of data points of the curve fit are less.

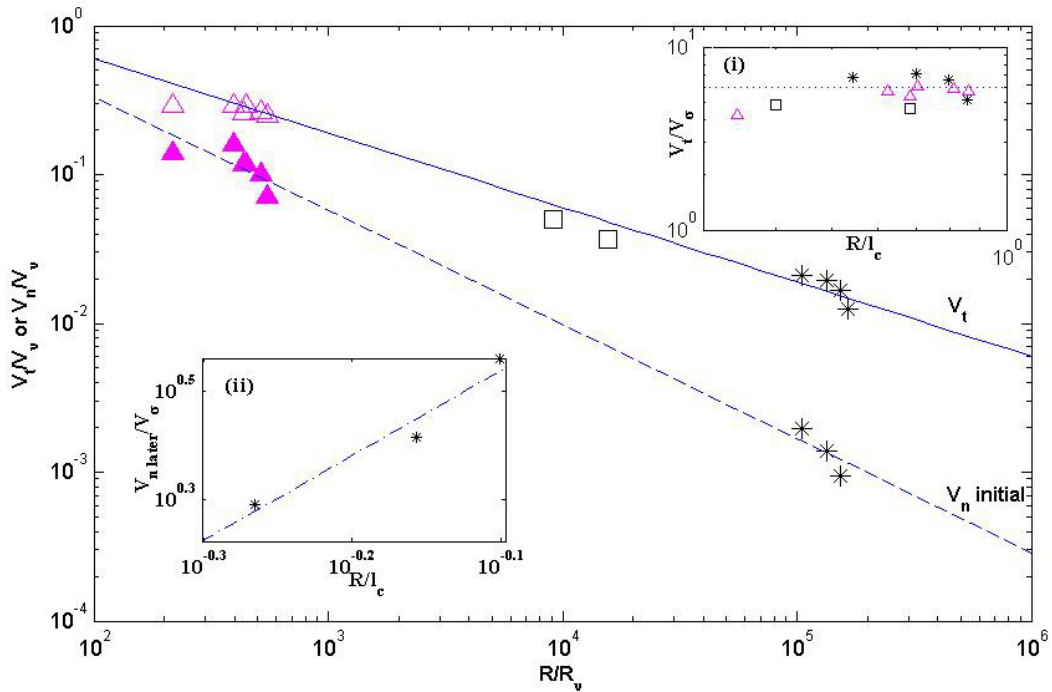


Fig 3: Variation of tangential velocity ( $V_t$ ) and normal velocity ( $V_n$ ) of the disturbance front with the bubble radius in dimensionless form. The capillary velocity scaling of  $V_t$  is shown in the inset (i). Dependence of  $V_n$ , obtained from the latter part of disturbance propagation, on the bubble radius in the inset (ii). \*, water;  $\Delta$ , GW 72;  $\square$ , ethanol; —,  $\frac{V_t}{V_v} = 6 \left(\frac{R}{R_v}\right)^{-1/2}$ ; ---,  $\frac{V_n}{V_v} = 11.44 \left(\frac{R}{R_v}\right)^{-0.77}$ ; ....,  $V_t = 6 V_\sigma$ ; - - - - ,  $\frac{V_n}{V_\sigma} = 4.96 \left(\frac{R}{l_c}\right)^{1.57}$ .

### 3.2. Total time for cavity collapse $t_{tc}$

We define the time between the emergence of the rim and the formation of the conical cavity as the total cavity collapse time  $t_{tc}$  (Fig 2(b) to Fig 2(m)). Fig 4 shows the variation of dimensionless  $t_{tc}$  against dimensionless bubble radius  $R$ , where  $t_{tc}$  is normalised by  $t_v$ , the viscous capillary time and  $R$  is normalised by  $R_v$ .  $t_{tc}/t_v$  for all the bubbles of different radii in the different fluids obey the relation

$$\frac{t_{tc}}{t_v} = 0.287 \left(\frac{R}{R_v}\right)^{3/2} \text{ ---- (2).}$$

Equation (2) implies that  $t_{tc}=0.287 t_v$  as shown in the inset of Fig 4, in the range  $10^2 < R/R_v < 5 \times 10^5$ , where  $t_v = \left(\frac{\rho}{\sigma}\right)^{1/2} R^{3/2}$  is the capillary time scale. No change in the trend of the curve in Fig 4, is seen around  $R/R_v \approx 10^3$  as in the case of the variation  $V/V_v$  with  $R/R_v$  shown by [9], where  $V$  is the jet velocity at free surface. Hence, it appears that the viscous cut off for the jet velocity may not be due to a similar viscous regime in the collapse of the cavity since no such viscous dependence in the overall cavity dynamics is seen in Fig 4 in the regime of our concern. Therefore,

it needs to be studied whether viscous effects become important after the cavity reaches a conical shape.

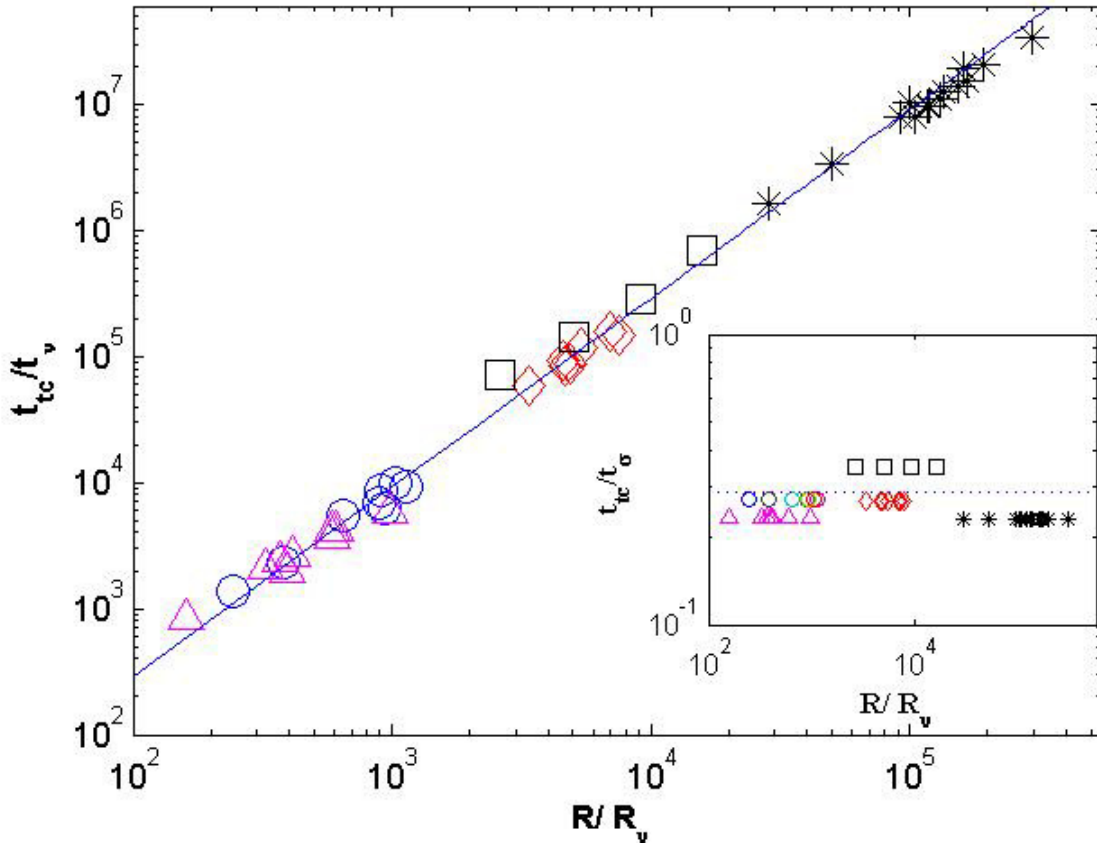


Fig 4: Variation of dimensionless collapse time of the cavity ( $t_{tc}$ ) with the dimensionless bubble radius ( $R$ ).  $t_{tc}$  is normalised with viscous capillary time scale  $t_v$  and the bubble radius is normalised with viscous capillary length  $R_v$ . The inset shows that  $t_{tc}$  scales as  $t_\sigma$ , the capillary time scale. \*, water; O, GW 68;  $\Delta$ , GW 72;  $\diamond$ , 2-propanol;  $\square$ , ethanol; —,  $\frac{t_{tc}}{t_v} = 0.287 \left(\frac{R}{R_v}\right)^{3/2}$ ; ....,  $t_{tc} = 0.287 t_\sigma$

### 3.3. Cavity filling rate

The filling rate of the cavity is calculated by measuring the displacement of the free surface contours from the images and assuming that the same displacement occurs everywhere azimuthally. Fig 5 shows the interface contours at successive time instants, superimposed over each other. We notice that the filling of the cavity has two contributions, (a) flow from sides  $Q_s$  which is predominantly radially inwards and is due to the change in the interfacial shape after the disturbance front has passed; (b)  $Q_b$  due to shrinking and rising of the undisturbed, concave cavity surface. Fig 6 shows,  $Q_s$ , and  $Q_t = Q_s + Q_b$  as a function of time for bubbles produced in water.  $Q_t$  is approximately constant until the cone formation, after which  $Q_t$  decreases linearly. This decrease in  $Q_t$  towards the later part could be because of the jet formation which results in part of the fluid being fed into the jet. The side discharge is found to be increasing with time possibly because the region of radial displacement behind the

disturbance increases as the disturbance travels down along the cavity surface with a velocity  $V_t$ .

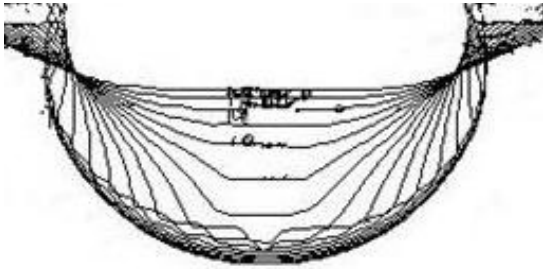


Fig 5: Superimposed contours of cavity collapse for  $R=2.15\text{mm}$  in water. Contours are separated by 0.25 milli seconds.

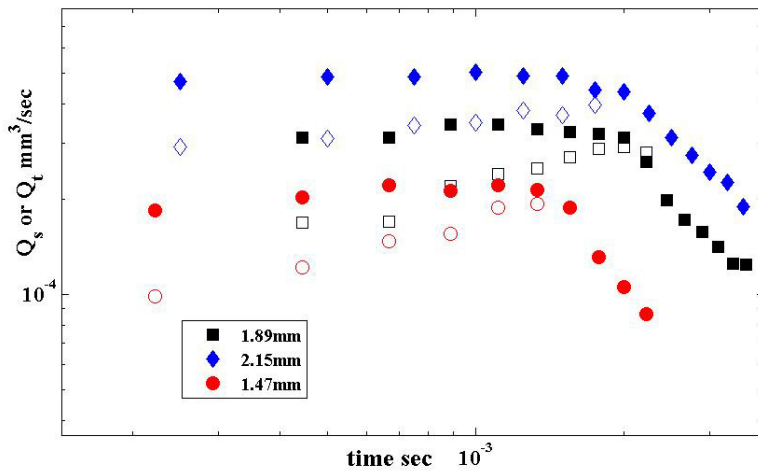


Fig 6: variation of the measured filling rate of cavity with time, for bubbles in water. Open markers represent the radial discharge  $Q_s$  and the filled markers represent the total discharge  $Q_t$ .

### 3.4. Curvature of disturbed cavity surface

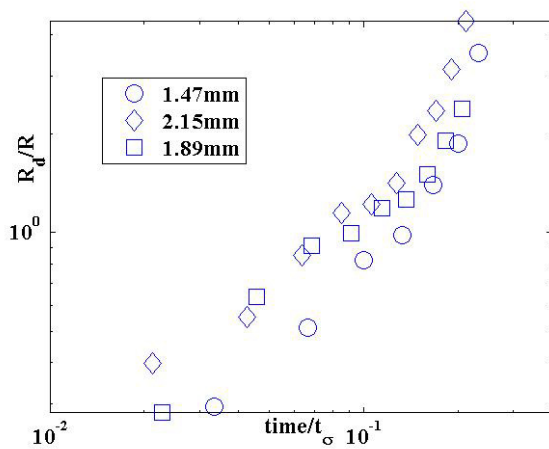


Fig 7: Variation of dimensionless cavity curvature ( $R_d$ ) against dimensionless time, measured for bubbles in water.

We fit a circular arc to the disturbed part of the cavity surface behind the disturbance front which is convex in shape to study the evolution of the radius of this part ( $R_d$ ) with time; Fig 2(f) shows the variation of  $R_d$  with time. Fig 7 shows the variation of dimensionless  $R_d$  against dimensionless time, where  $R_d$  is normalised by bubble radius  $R$  and time is normalised by the capillary time scale  $t_\sigma$ . The radius evolution showed two regimes. Till  $t/t_\sigma \approx 0.15$ ,  $R_d/R = 5 (t/t_\sigma)^{0.747}$ , while after that  $R_d/R = 80(t/t_\sigma)^{2.123}$ . More measurements need to be carried out to confirm the dependence of  $R_d$  with time.

## Conclusion

The dynamics of collapse of a cavity created at the free surface due to a bubble was studied in this paper. The time taken for the completion of cavity collapse  $t_{ic}$  was measured for bubbles of different sizes in five different fluids and found to scale as  $t_{ic} = 0.287 \left(\frac{\rho}{\sigma}\right)^{1/2} R^{3/2}$ , in the range  $10^2 < R/R_v < 5 \times 10^5$ , where  $R_v$  is the viscous capillary length scale. The above relation implies that the cavity collapse is dominated by surface tension and inertial forces and the role of viscosity seems negligible. This contrasts with the viscous cut off observed for jet velocity around  $R/R_v \approx 10^3$  by [9]. Velocity of the disturbance front was resolved in the tangential and the normal direction to the undisturbed interface. The tangential velocity throughout the collapse was constant for given bubble radius in any fluid and obeyed the relation  $V_t = 6 \sqrt{\frac{\sigma}{\rho R}}$ , that is six times the capillary velocity, in the range  $10^2 < R/R_v < 2 \times 10^5$ . The normal velocity of the disturbance had two regimes; in the initial part of the disturbance  $\frac{V_n}{V_v} = 11.44 \left(\frac{R}{R_v}\right)^{-0.77}$  while the latter part it scaled as  $\frac{V_n}{V_\sigma} = 4.96 \left(\frac{R}{R_c}\right)^{1.57}$ . A study of cavity filling rate showed that the rate of filling the cavity is a constant till the cavity turns itself into a conical surface. The evolution of cavity curvature  $R_d$  was studied. Two different regimes were visible; till  $t/t_\sigma \approx 0.15$ ,  $R_d/R = 5 (t/t_\sigma)^{0.747}$ , after that  $R_d/R = 80(t/t_\sigma)^{2.123}$ .

## References

1. Boulton-Stone, J. M. and Blake, J. R. 1993 Gas bubbles bursting at a free surface. *J. Fluid Mech.* 254, 437-466.
2. Clanet, C., and Lasheras, J. C. 1999 Transition from dripping to jetting. *J. Fluid Mech.* 383, 307-326.
3. Das, S. P., Hopfinger, E. J. 2008 Parametrically forced gravity waves in a circular cylinder and finite- time singularity *J. Fluid Mech.* 599, 205-228.
4. Duchemin, L., Popinet, S., Josserand, C. and Zaleski, S. 2002 Jet formation in bubbles bursting at a free surface. *POF.* 14, 3000-3008.
5. Kientzler, C.F., Arons, A. B., Blanchard, D. C. and Woodcock, A. H. 1954 Photographic investigation of the projection of droplets by bubbles bursting at a water surface. *Tellus.* 6, 1-7.
6. Longuet-Higgins, M. S. 1983 Bubbles, breaking waves and hyperbolic jets at a free surface. *J. Fluid. Mech.* 127, 103-121.
7. Lhuissier, H. and Villermaux, E. 2012 Bursting bubble aerosols. *J. Fluid. Mech.* 696, 5-44.
8. MacIntyre, F. 1972 Flow patterns in breaking bubbles. *J. Geophy. Res.* 77, 5211-5228.
9. Sangeeth, K, Puthenveettil, B. A., and Hopfinger, E. J.. Jet formation from bubble collapse at a free surface. XXIII ICTAM, 19-24 August 2012, Beijing, China
10. Zeff, B. W., Kleber, B., Fineberg, J. and Lathrop, D. P. 2000 Singularity dynamics in curvature collapse and jet eruption on a fluid surface. *Nature.* 403, 401-404.